Proposal for Numerical Benchmarking of Fluid–Structure Interaction Between an Elastic Object and Laminar Incompressible Flow

Chapter · June 2007

DOI: 10.1007/3-540-34596-5_15

2 authors:

Stefan Turek
TU Dortmund University
349 PUBLICATIONS **12,360** CITATIONS

SEE PROFILE

Jaroslav Hron
Charles University in Prague
77 PUBLICATIONS **2,847** CITATIONS

SEE PROFILE

Proposal for numerical benchmarking of fluid-structure interaction between an elastic object and laminar incompressible flow

Stefan Turek and Jaroslav Hron*

Institute for Applied Mathematics and Numerics, University of Dortmund, Vogelpothsweg 87, 44227 Dortmund, Germany

Abstract. We describe new benchmark settings for the rigorous evaluation of different methods for fluid-structure interaction problems. The configurations consist of laminar incompressible channel flow around an elastic object which results in self-induced oscillations of the structure. Moreover, characteristic flow quantities and corresponding plots are provided for a quantitative comparison.

1 Introduction

The main purpose of this benchmark proposal is to describe specific configurations which shall help in future to test and to compare different numerical methods and code implementations for the fluid-structure interaction (FSI) problem. In particular, the various coupling mechanisms, ranging from partitioned, weakly coupled approaches to fully coupled, monolithic schemes are of high interest. Moreover, it shall be possible to examine the quality of different discretization schemes (FEM, FV, FD, LBM, resp., beam, shell, volume elements), and the robustness and numerical efficiency of the integrated solver components shall be a further aspect. This new benchmark is based on the older successful *flow around cylinder* setting developed in [3] for incompressible laminar flow and on the setup in [4]. Similar to these older configurations we consider the fluid to be incompressible and in the laminar regime. The structure is allowed to be compressible, and the deformations of the structure should be significant. The overall setup of the interaction problem is such that the solid object with elastic part is submerged in a channel flow. Then, self induced oscillations in the fluid and the deformable part of the structure are obtained so that characteristic physical quantities and plots for the time-dependent results can be provided.

* with support by M. Schäfer, M. Heck, S. Yigit, M. Krafczyk, J. Tölke, S. Geller, H.-J. Bungartz, M. Brenk, R. Rannacher, T. Dunne, W. Wall, A. Gerstenberger, P. Gamnitzer, E. Rank, A. Düster, S. Kollmannsberger, D. Scholz, F. Durst, H. Lienhart, J. Gomes, K.-U. Bletzinger, A. Kupzok, R. Wüchner
This work has been supported by German Reasearch Association (DFG), Reasearch unit 493.

2 Definitions

We consider the flow of an **incompressible Newtonian fluid** interacting with an **elastic solid**. We denote by Ω_t^f the domain occupied by the fluid and Ω_t^s by the solid at the time $t \in [0, T]$. Let $\Gamma_t^0 = \bar{\Omega}_t^f \cap \bar{\Omega}_t^s$ be the part of the boundary where the elastic solid interacts with the fluid.

2.1 Fluid properties

The fluid is considered to be **Newtonian**, **incompressible** and its state is described by the velocity and pressure fields $\boldsymbol{v}^f, p^f$. The balance equations are

$$\begin{aligned} \varrho^f \frac{\partial \boldsymbol{v}^f}{\partial t} + \varrho^f (\nabla \boldsymbol{v}^f)\boldsymbol{v}^f &= \operatorname{div} \boldsymbol{\sigma}^f \qquad \text{in } \Omega_t^f. \\ \operatorname{div} \boldsymbol{v}^f &= 0 \end{aligned} \tag{1}$$

The material constitutive equation is

$$\boldsymbol{\sigma}^f = -p^f \boldsymbol{I} + \varrho^f \nu^f (\nabla \boldsymbol{v}^f + \nabla \boldsymbol{v}^{f\,\mathrm{T}}). \tag{2}$$

The constant density of the fluid is ϱ^f and the viscosity is denoted by ν^f. The Reynolds number is defined by $\mathrm{Re} = \frac{2r\bar{V}}{\nu^f}$, with the mean velocity $\bar{V} = \frac{2}{3}v(0, \frac{H}{2}, t)$, r radius of the cylinder and H height of the channel (see Fig. 1).

2.2 Structure properties

The structure is assumed to be **elastic** and **compressible**. Its configuration is described by the displacement $\boldsymbol{u}^s$, with velocity field $\boldsymbol{v}^s = \frac{\partial \boldsymbol{u}^s}{\partial t}$. The balance equations are

$$\varrho^s \frac{\partial \boldsymbol{v}^s}{\partial t} + \varrho^s (\nabla \boldsymbol{v}^s)\boldsymbol{v}^s = \operatorname{div}(\boldsymbol{\sigma}^s) + \varrho^s \boldsymbol{g} \qquad \text{in } \Omega_t^s. \tag{3}$$

Written in the more common Lagrangian description, i.e. with respect to some fixed reference (initial) state Ω^s, we have

$$\varrho^s \frac{\partial^2 \boldsymbol{u}^s}{\partial t^2} = \operatorname{div}(J\boldsymbol{\sigma}^s \boldsymbol{F}^{-\mathrm{T}}) + \varrho^s \boldsymbol{g} \qquad \text{in } \Omega^s \tag{4}$$

where $\boldsymbol{F} = \boldsymbol{I} + \nabla \boldsymbol{u}^s$ is the deformation gradient tensor. For further details see for example [1].

The material is specified by giving the Cauchy stress tensor $\boldsymbol{\sigma}^s$ (the 2nd Piola-Kirchhoff stress tensor is then given by $\boldsymbol{S}^s = J\boldsymbol{F}^{-1}\boldsymbol{\sigma}^s\boldsymbol{F}^{-T}$) by the

following constitutive law for the **St. Venant-Kirchhoff** material ($\boldsymbol{E} = \frac{1}{2}(\boldsymbol{F}^{\mathrm{T}}\boldsymbol{F} - \boldsymbol{I})$)

$$\boldsymbol{\sigma}^s = \frac{1}{J}\boldsymbol{F}\left(\lambda^s(\mathrm{tr}\,\boldsymbol{E})\boldsymbol{I} + 2\mu^s\boldsymbol{E}\right)\boldsymbol{F}^{\mathrm{T}} \tag{5}$$

$$\boldsymbol{S}^s = \lambda^s(\mathrm{tr}\,\boldsymbol{E})\boldsymbol{I} + 2\mu^s\boldsymbol{E} \tag{6}$$

The density of the structure in the undeformed configuration is ϱ^s. The elasticity of the material is characterized by the Poisson ratio ν^s ($\nu^s < \frac{1}{2}$ for a compressible structure) and by the Young modulus E. The alternative characterization is described by the Lamé coefficients λ^s and μ^s (the shear modulus):

$$\nu^s = \frac{\lambda^s}{2(\lambda^s + \mu^s)} \qquad E = \frac{\mu^s(3\lambda^s + 2\mu^s)}{(\lambda^s + \mu^s)} \tag{7}$$

$$\mu^s = \frac{E}{2(1+\nu^s)} \qquad \lambda^s = \frac{\nu^s E}{(1+\nu^s)(1-2\nu^s)} \tag{8}$$

2.3 Interaction conditions

The boundary conditions on the fluid solid interface are assumed to be

$$\begin{aligned} \boldsymbol{\sigma}^f\boldsymbol{n} &= \boldsymbol{\sigma}^s\boldsymbol{n} \\ \boldsymbol{v}^f &= \boldsymbol{v}^s \end{aligned} \qquad \text{on } \Gamma_t^0, \tag{9}$$

where $\boldsymbol{n}$ is a unit normal vector to the interface Γ_t^0. This implies the no-slip condition for the flow, and that the forces on the interface are in balance.

2.4 Domain definition

The domain is based on the 2D version of the well-known CFD benchmark in [3] and shown here in Figure 1. By omitting the elastic bar behind the cylinder one can exactly recover the setup of the *flow around cylinder* configuration which allows for validation of the flow part by comparing the results with the older flow benchmark.

- The domain dimensions are: length $L = 2.5$, height $H = 0.41$.
- The circle center is positioned at $C = (0.2, 0.2)$ (measured from the left bottom corner of the channel) and the radius is $r = 0.05$.
- The elastic structure bar has length $l = 0.35$ and height $h = 0.02$, the right bottom corner is positioned at $(0.6, 0.19)$, and the left end is fully attached to the fixed cylinder.
- The control points are $A(t)$, fixed with the structure with $A(0) = (0.6, 0.2)$, and $B = (0.15, 0.2)$.

The setting is intentionally non-symmetric (see [3]) to prevent the dependence of the onset of any possible oscillation on the precision of the computation.

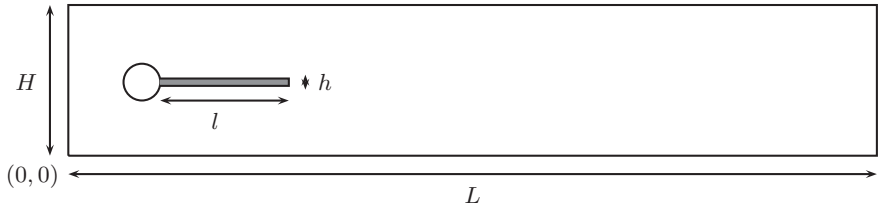

Fig. 1. Computational domain

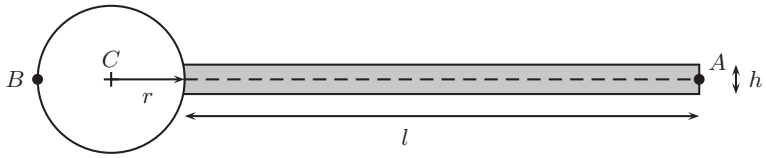

Fig. 2. Detail of the structure part

2.5 Boundary conditions

- A parabolic velocity profile is prescribed at the left channel inflow

$$v^f(0,y) = 1.5\bar{U}\frac{y(H-y)}{\left(\frac{H}{2}\right)^2} = 1.5\bar{U}\frac{4.0}{0.1681}y(0.41-y), \tag{10}$$

  such that the mean inflow velocity is $\bar{U}$ and the maximum of the inflow velocity profile is $1.5\bar{U}$.
- The outflow condition can be chosen by the user, for example *stress free* or *do nothing* conditions. The outflow condition effectively prescribes some reference value for the pressure variable p. While this value could be arbitrarily set in the incompressible case, in the case of compressible structure this will have influence on the stress and consequently the deformation of the solid. In this proposal, we set the reference pressure at the outflow to have *zero mean value*.
- The *no-slip* condition is prescribed for the fluid on the other boundary parts. i.e. top and bottom wall, circle and fluid-structure interface Γ_t^0.

2.6 Initial conditions

Suggested starting procedure for the non-steady tests is to use a smooth increase of the velocity profile in time as

$$v^f(t,0,y) = \begin{cases} v^f(0,y)\frac{1-\cos(\frac{\pi}{2}t)}{2} & \text{if } t < 2.0 \\ v^f(0,y) & \text{otherwise} \end{cases} \tag{11}$$

where $v^f(0,y)$ is the velocity profile given in (10).

geometry parameters		value [m]
channel length	L	2.5
channel width	H	0.41
cylinder center position	C	$(0.2, 0.2)$
cylinder radius	r	0.05
elastic structure length	l	0.35
elastic structure thickness	h	0.02
reference point (at $t = 0$)	A	$(0.6, 0.2)$
reference point	B	$(0.2, 0.2)$

Table 1. Overview of the geometry parameters

2.7 Material parameters

material	ϱ^s $[\frac{\text{kg}}{\text{m}^3}]$	ν^s	E $[10^6 \frac{\text{kg}}{\text{ms}^2}]$	μ^s $[10^6 \frac{\text{kg}}{\text{ms}^2}]$
polybutadiene	910	0.50	1.6	0.53
polyurethane	1200	0.50	25	8.3
polypropylene	1100	0.42	900	317
PVC	1400	0.42	1500	528
steel	7800	0.29	210000	81400
cork	180	0.25	32	12.8

material	ϱ^f $[\frac{\text{kg}}{\text{m}^3}]$	ν^f $[10^{-6} \frac{\text{m}^2}{\text{s}}]$	μ^f $[10^{-3} \frac{\text{kg}}{\text{ms}}]$
air	1.23	0.015	0.018
aceton	790	0.405	0.32
ethyl alcohol	790	1.4	1.1
oil, vegetable	920	76.1	70
water	1000	1.14	1.14
blood	1035	$3 - 4$	$3 - 4$
glycerine	1260	1127	1420
honey	1420	7042	10000
mercury	13594	0.0114	1.55

Table 2. Overview of some solid and fluid material parameters (densities ϱ^f, ϱ^s, Poisson ratio ν^s, Young modulus E, shear modulus μ^s, dynamic viscosity μ^f and kinematic viscosity ν^f)

An overview of certain material properties for some relevant fluids and elastic materials is shown in the Table 2. The choice of the parameters for the benchmark is guided by several requirements:

First, we would like the flow to be in the laminar regime, which implies "small" Reynolds numbers. On the other hand, the flow should be capable of deforming the elastic structure. A typical fluid candidate for such experiments is glycerine.

parameter	polybutadiene & glycerine	polypropylene & glycerine
ϱ^s $[10^3 \frac{\mathrm{kg}}{\mathrm{m}^3}]$	0.91	1.1
ν^s	0.5	0.42
μ^s $[10^6 \frac{\mathrm{kg}}{\mathrm{ms}^2}]$	0.53	317
ϱ^f $[10^3 \frac{\mathrm{kg}}{\mathrm{m}^3}]$	1.26	1.26
ν^f $[10^{-3} \frac{\mathrm{m}^2}{\mathrm{s}}]$	1.13	1.13

Table 3. Proposed material combination

In order not to introduce additional numerical complications connected with high aspect ratios in the geometry, the deformable structure has a certain thickness which requires that the stiffness of the material should be low enough to allow significant deformations. Certain rubber-like materials fit into such a setting, namely polybutadiene (for a future incompressible configuration) and polypropylene.

In Table 3 the material parameters are presented for 2 combinations of glycerine and selected rubber-like material.

3 Quantities for comparison

According to our preliminary calculations, self induced periodic oscillations develop in the flow and structure. The comparison will be done for *fully developed flow*, and particularly for *one full period of the oscillation* with respect to the position of the point $A(t)$. The suggested quantities of interest are:

1. The y-coordinate $y(t)$ of the end of the beam structure at point $A(t)$ (see the Figure 2).
2. Forces exerted by the fluid on the *whole* submerged body, i.e. lift and drag forces acting on the cylinder and the beam structure together

$$(F_D, F_L) = \int_S \boldsymbol{\sigma} \boldsymbol{n} dS,$$

where $S = S_1 \cup S_2$ (see Fig. 3) denotes the part of the circle being in contact with the fluid (i.e. S_1) plus part of the boundary of the beam structure being in contact with the fluid (i.e. S_2), and $\boldsymbol{n}$ is the outer unit normal vector to the integration path with respect to the fluid domain.

Remark 1. The forces can be calculated in several different ways, i.e.

$$\begin{aligned}(F_D, F_L) = \int_S \boldsymbol{\sigma}\boldsymbol{n}dS &= \int_{S_1} \boldsymbol{\sigma}^f \boldsymbol{n}dS + \int_{S_2} \boldsymbol{\sigma}^f \boldsymbol{n}dS \\ &= \int_{S_1} \boldsymbol{\sigma}^f \boldsymbol{n}dS + \int_{S_2} \boldsymbol{\sigma}^s \boldsymbol{n}dS \\ &= \int_{S_1} \boldsymbol{\sigma}^f \boldsymbol{n}dS + \int_{S_2} \frac{1}{2}(\boldsymbol{\sigma}^s + \boldsymbol{\sigma}^f)\boldsymbol{n}dS \\ &= \int_{S_0} \boldsymbol{\sigma}\boldsymbol{n}dS.\end{aligned}$$

That means that, up to numerical effects, all proposed evaluations will lead (asymptotically) to the same results.

3. Pressure difference between the points $A(t)$ and B

$$\Delta p^{AB} = p^B - p^{A(t)}.$$

The position of the point $A(t)$ is time dependent.

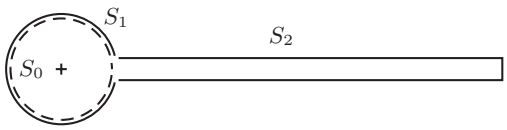

Fig. 3. Integration path $S = S_1 \cup S_2$ for the force calculation

The time dependent values are represented by the mean value, amplitude and frequency. The mean value and amplitude are computed from the last period of the oscillations by taking the maximum and minimum values, then the mean value is taken as average of the min/max values, and the amplitude is the difference of the max/min from the mean:

$$\begin{aligned}\text{mean} &= \frac{1}{2}(\max + \min) \\ \text{amplitude} &= \frac{1}{2}(\max - \min)\end{aligned}$$

The frequency of the oscillations can be computed either from the period time T as

$$\text{frequency} = \frac{1}{T}$$

or by using fourier analysis on the periodic data and taking the lowest significant frequency present in the spectrum. Additionally, a plot of the quantities over the period should be presented.

4 Partial computational tests

For the validation of the employed fluid and solid solvers, we first describe partial tests which are performed on different levels of mesh refinement (see Fig. and Table 4) with various time steps. We provide the results for the different discretization levels in the following since these sequences of results indicate that our given "reference results" are almost grid-independent. All simulations have been performed with a fully implicit monolithic ALE-FEM method with a fully coupled multigrid solver as described in [2].

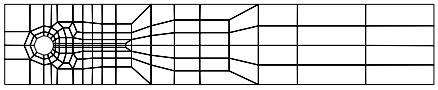

level	#refine	#el	#dof
0+0	0	62	1338
1+0	1	248	5032
2+0	2	992	19488
3+0	3	3968	76672
4+0	4	15872	304128

Fig. 4. Example of a coarse mesh and the number of degrees of freedom for refined levels

4.1 CFD tests

Taking the flag as a rigid object, we perform 3 subtests focusing on the fluid dynamics part of the problem. The flag can be made almost rigid by setting the structural parameters to large values ($\varrho^s = 10^6 \frac{\text{kg}}{\text{m}^3}, \mu^s = 10^{12} \frac{\text{kg}}{\text{ms}^2}$) or completely rigid by considering the flow domain only with fixed boundary conditions on the flag interface.

dimensional parameter	CFD1	CFD2	CFD3
ϱ^f $[10^3 \frac{\text{kg}}{\text{m}^3}]$	1	1	1
ν^f $[10^{-3} \frac{\text{m}^2}{\text{s}}]$	1	1	1
U $[\frac{\text{m}}{\text{s}}]$	0.2	1	2
non-dimensional parameter	**CFD1**	**CFD2**	**CFD3**
$\text{Re} = \frac{Ud}{\nu^f}$	20	100	200
$\bar{U}$	0.2	1	2

Table 4. Parameter settings for the CFD tests

level	nel	ndof	drag	lift
$0+0$	144	3032	$1.41635 \times 10^{+01}$	$1.15592 \times 10^{+00}$
$1+0$	576	11536	$1.42236 \times 10^{+01}$	$1.11747 \times 10^{+00}$
$2+0$	2304	44960	$1.42730 \times 10^{+01}$	$1.11692 \times 10^{+00}$
$3+0$	9216	177472	$1.42880 \times 10^{+01}$	$1.11852 \times 10^{+00}$
$4+0$	36864	705152	$1.42919 \times 10^{+01}$	$1.11896 \times 10^{+00}$
$5+0$	147456	2811136	$1.42927 \times 10^{+01}$	$1.11904 \times 10^{+00}$
$5+1$	150528	2869504	$1.42929 \times 10^{+01}$	$1.11906 \times 10^{+00}$
$5+2$	156672	2986240	$1.42929 \times 10^{+01}$	$1.11905 \times 10^{+00}$
$5+3$	168960	3219712	$1.42929 \times 10^{+01}$	$1.11905 \times 10^{+00}$
$6+0$	589824	11225600	$1.42929 \times 10^{+01}$	$1.11905 \times 10^{+00}$
ref.			14.29	1.119

Table 5. Results for **CFD1**

level	nel	ndof	drag	lift
$0+0$	144	3032	$1.33188 \times 10^{+02}$	$1.18522 \times 10^{+01}$
$1+0$	576	11536	$1.34996 \times 10^{+02}$	$1.10739 \times 10^{+01}$
$2+0$	2304	44960	$1.36355 \times 10^{+02}$	$1.05337 \times 10^{+01}$
$3+0$	9216	177472	$1.36610 \times 10^{+02}$	$1.05303 \times 10^{+01}$
$4+0$	36864	705152	$1.36678 \times 10^{+02}$	$1.05347 \times 10^{+01}$
$5+0$	147456	2811136	$1.36696 \times 10^{+02}$	$1.05349 \times 10^{+01}$
$5+1$	150528	2869504	$1.36700 \times 10^{+02}$	$1.05346 \times 10^{+01}$
$5+2$	156672	2986240	$1.36701 \times 10^{+02}$	$1.05343 \times 10^{+01}$
$5+3$	168960	3219712	$1.36701 \times 10^{+02}$	$1.05340 \times 10^{+01}$
$6+0$	589824	11225600	$1.36700 \times 10^{+02}$	$1.05343 \times 10^{+01}$
ref.			136.7	10.53

Table 6. Results for **CFD2**

CFD3: lift and drag forces on the cylinder+flag

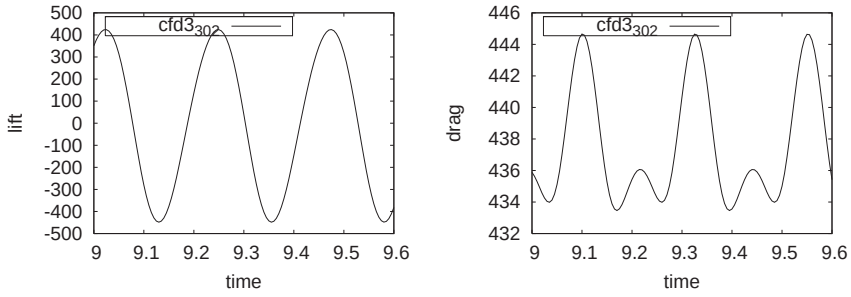

level	nel	ndof	drag	lift
$1+0$	576	11536	416.8 ± 3.3578[4.3825]	-24.702 ± 342.38[4.3825]
$2+0$	2304	44960	437.29 ± 5.3462[4.3825]	-11.085 ± 429.88[4.3825]
$3+0$	9216	177472	438.99 ± 5.4419[4.3825]	-10.289 ± 433.09[4.3825]
$4+0$	36864	705152	439.38 ± 5.4639[4.3825]	-9.9868 ± 434.79[4.3825]
level	nel	ndof	drag	lift
$1+0$	576	11536	416.83 ± 3.4023[4.3956]	-23.897 ± 346.72[4.3956]
$2+0$	2304	44960	437.41 ± 5.5856[4.3956]	-12.673 ± 434.74[4.3956]
$3+0$	9216	177472	439.05 ± 5.5804[4.3956]	-11.837 ± 436.17[4.3956]
$4+0$	36864	705152	439.45 ± 5.6183[4.3956]	-11.893 ± 437.81[4.3956]
ref.			439.45 ± 5.6183[4.3956]	-11.893 ± 437.81[4.3956]

Table 7. Results for **CFD3** with $\Delta t = 0.01$ and 0.005

4.2 CSM tests

The structural tests are computed only for the elastic beam (without the surrounding fluid) adding the gravitational force *only*(!) on the structural part, $\boldsymbol{g} = (0, g)$ $[\frac{\mathrm{m}}{\mathrm{s}^2}]$. The CSM3 test is computed as a time dependent case starting from the undeformed configuration while the tests CSM1 and CSM2 are the steady state solutions.

par. dim.	CSM1	CSM2	CSM3
ϱ^s $[10^3 \frac{\mathrm{kg}}{\mathrm{m}^3}]$	1	1	1
ν^s	0.4	0.4	0.4
μ^s $[10^6 \frac{\mathrm{kg}}{\mathrm{ms}^2}]$	0.5	2.0	0.5
ϱ^f $[10^3 \frac{\mathrm{kg}}{\mathrm{m}^3}]$	1	1	1
ν^f $[10^{-3} \frac{\mathrm{m}^2}{\mathrm{s}}]$	1	1	1
U $[\frac{\mathrm{m}}{\mathrm{s}}]$	0	0	0
g $[\frac{\mathrm{m}}{\mathrm{s}^2}]$	2	2	2
par. non-dim.	CSM1	CSM2	CSM3
$\beta = \frac{\varrho^s}{\varrho^f}$	1	1	1
ν^s	0.4	0.4	0.4
E^s $[\frac{\mathrm{kg}}{\mathrm{ms}^2}]$	1.4×10^6	5.6×10^6	1.4×10^6
$\mathrm{Re} = \frac{Ud}{\nu^f}$	0	0	0
$\bar{U}$	0	0	0
g	2	2	2

Table 8. Parameter settings for the CSM tests

level	nel	ndof	ux of A $[\times 10^{-3}]$	uy of A $[\times 10^{-3}]$
$2+0$	320	6468	-7.17301	-66.0263
$3+0$	1280	25092	-7.18372	-66.0817
$4+0$	5120	98820	-7.18656	-66.0965
$4+1$	6260	120512	-7.18738	-66.1008
$4+2$	8552	164092	-7.18766	-66.1023
$4+3$	13148	251448	-7.18777	-66.1029
$5+0$	20480	392196	-7.18739	-66.1009
$5+1$	22772	435776	-7.18767	-66.1023
ref.			-7.187	-66.10

Table 9. Results for **CSM1**

level	nel	ndof	ux of A $[\times 10^{-3}]$	uy of A $[\times 10^{-3}]$
$2+0$	320	6468	-0.468011	-16.9536
$3+0$	1280	25092	-0.468734	-16.9684
$4+0$	5120	98820	-0.468925	-16.9723
$4+1$	6260	120512	-0.468980	-16.9735
$4+2$	8552	164092	-0.468999	-16.9739
$4+3$	13148	251448	-0.469006	-16.9740
$5+0$	20480	392196	-0.468981	-16.9735
$5+1$	22772	435776	-0.469000	-16.9739
ref			-0.4690	-16.97

Table 10. Results for **CSM2**

CSM3: The displacement of the point A

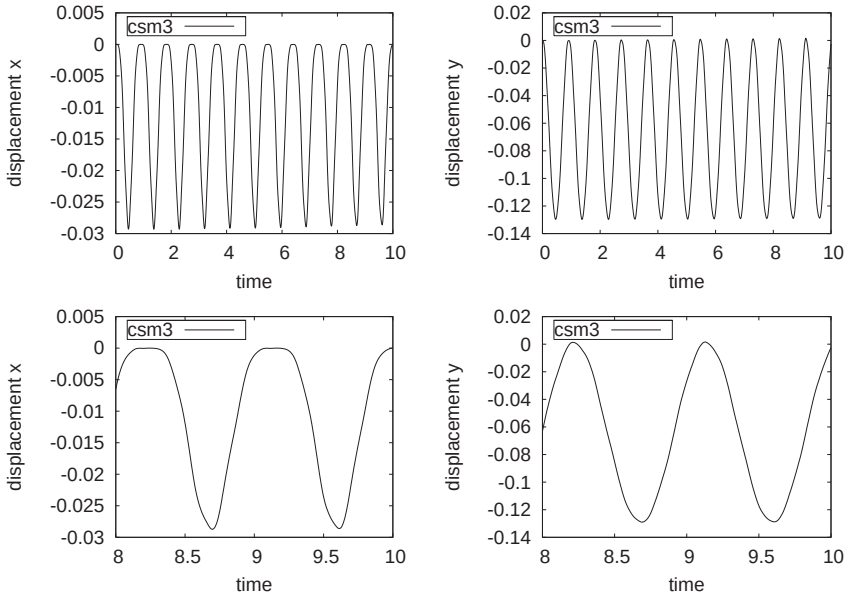

level	nel	ndof	ux of A $[\times 10^{-3}]$	uy of A $[\times 10^{-3}]$
$2+0$	320	6468	$-14.384 \pm 14.389[1.0956]$	$-64.271 \pm 64.595[1.0956]$
$3+0$	1280	25092	$-14.402 \pm 14.406[1.0956]$	$-64.352 \pm 64.679[1.0956]$
$4+0$	5120	98820	$-14.404 \pm 14.408[1.0956]$	$-64.371 \pm 64.695[1.0956]$
level	nel	ndof	ux of A $[\times 10^{-3}]$	uy of A $[\times 10^{-3}]$
$2+0$	320	6468	$-14.632 \pm 14.636[1.0978]$	$-64.744 \pm 64.907[1.0978]$
$3+0$	1280	25092	$-14.645 \pm 14.650[1.0978]$	$-64.765 \pm 64.946[1.0978]$
$4+0$	5120	98820	$-14.645 \pm 14.650[1.0978]$	$-64.766 \pm 64.948[1.0978]$
level	nel	ndof	ux of A $[\times 10^{-3}]$	uy of A $[\times 10^{-3}]$
$2+0$	320	6468	$-14.279 \pm 14.280[1.0995]$	$-63.541 \pm 65.094[1.0995]$
$3+0$	1280	25092	$-14.299 \pm 14.299[1.0995]$	$-63.594 \pm 65.154[1.0995]$
$4+0$	5120	98820	$-14.305 \pm 14.305[1.0995]$	$-63.607 \pm 65.160[1.0995]$
ref			$-14.305 \pm 14.305[1.0995]$	$-63.607 \pm 65.160[1.0995]$

Table 11. Results for **CSM3** with timesteps $\Delta t = 0.02, 0.01, 0.005$

4.3 FSI tests

The following FSI tests are performed for two different inflow speeds. FSI1 is resulting in a steady state solution, while the other two tests (FSI2, FSI3) result in periodic solutions and correspond to the final benchmark settings.

parameter	FSI1	FSI2	FSI3
ϱ^s $[10^3 \frac{\mathrm{kg}}{\mathrm{m}^3}]$	1	10	1
ν^s	0.4	0.4	0.4
μ^s $[10^6 \frac{\mathrm{kg}}{\mathrm{ms}^2}]$	0.5	0.5	2.0
ϱ^f $[10^3 \frac{\mathrm{kg}}{\mathrm{m}^3}]$	1	1	1
ν^f $[10^{-3} \frac{\mathrm{m}^2}{\mathrm{s}}]$	1	1	1
U $[\frac{\mathrm{m}}{\mathrm{s}}]$	0.2	1	2
parameter	FSI1	FSI2	FSI3
$\beta = \frac{\varrho^s}{\varrho^f}$	1	10	1
ν^s	0.4	0.4	0.4
$\mathrm{Ae} = \frac{E^s}{\varrho^f \bar{U}^2}$	3.5×10^4	1.4×10^3	1.4×10^3
$\mathrm{Re} = \frac{\bar{U}d}{\nu^f}$	20	100	200
$\bar{U}$	0.2	1	2

Table 12. Parameter settings for the full FSI benchmarks

level	nel	ndof	ux of A $[\times 10^{-3}]$	uy of A $[\times 10^{-3}]$	drag	lift
$2+0$	992	19488	0.022871	0.81930	14.27360	0.76178
$3+0$	3968	76672	0.022775	0.82043	14.29177	0.76305
$4+0$	15872	304128	0.022732	0.82071	14.29484	0.76356
$5+0$	63488	1211392	0.022716	0.82081	14.29486	0.76370
$6+0$	253952	4835328	0.022708	0.82086	14.29451	0.76374
ref.			0.0227	0.8209	14.295	0.7638

Table 13. Results for **FSI1**

FSI2: x & y displacement of the point A

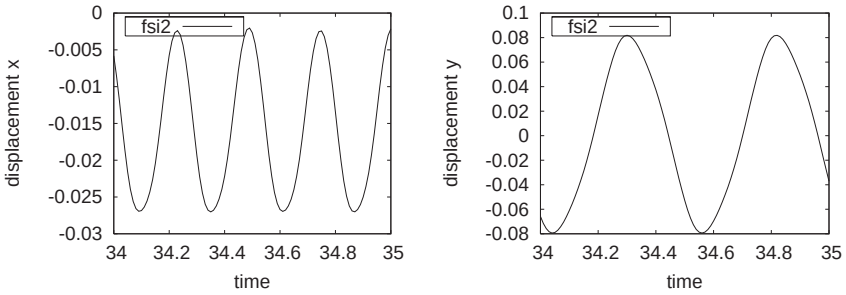

FSI2: lift and drag force on the cylinder+flag

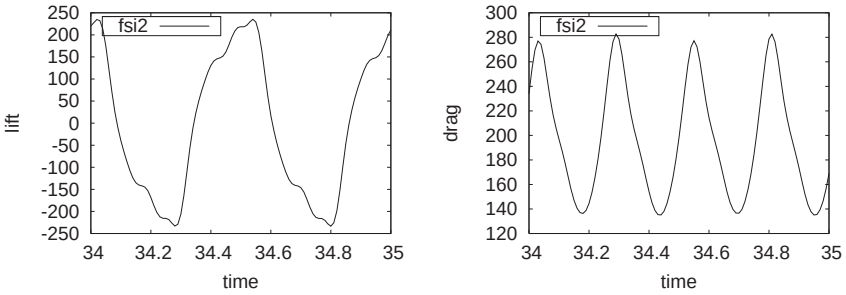

lev.	ux of A $[\times 10^{-3}]$	uy of A $[\times 10^{-3}]$	drag	lift
2	$-14.00 \pm 12.03[3.8]$	$1.18 \pm 78.7[2.0]$	$209.46 \pm 72.30[3.8]$	$-1.18 \pm 269.6[2.0]$
3	$-14.25 \pm 12.03[3.8]$	$1.20 \pm 79.2[2.0]$	$202.55 \pm 67.02[3.8]$	$0.71 \pm 227.1[2.0]$
4	$-14.58 \pm 12.37[3.8]$	$1.25 \pm 80.7[2.0]$	$201.29 \pm 67.61[3.8]$	$0.97 \pm 233.2[2.0]$
lev.	ux of A $[\times 10^{-3}]$	uy of A $[\times 10^{-3}]$	drag	lift
2	$-14.15 \pm 12.23[3.7]$	$1.18 \pm 78.8[1.9]$	$210.36 \pm 70.28[3.7]$	$0.80 \pm 286.0[1.9]$
3	$-13.97 \pm 12.01[3.8]$	$1.25 \pm 79.3[2.0]$	$203.54 \pm 68.43[3.8]$	$0.41 \pm 229.3[2.0]$
4	$-14.58 \pm 12.44[3.8]$	$1.23 \pm 80.6[2.0]$	$208.83 \pm 73.75[3.8]$	$0.88 \pm 234.2[2.0]$
ref.	$-14.58 \pm 12.44[3.8]$	$1.23 \pm 80.6[2.0]$	$208.83 \pm 73.75[3.8]$	$0.88 \pm 234.2[2.0]$

Table 14. Results for **FSI2** with timestep $\Delta t = 0.002, \Delta t = 0.001$

FSI3: x & y displacement of the point A

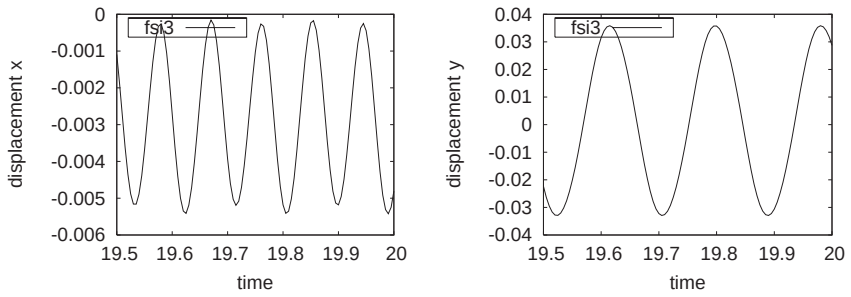

FSI3: lift and drag force on the cylinder+flag

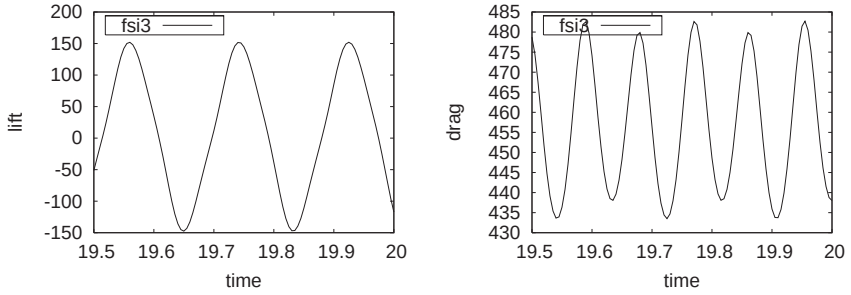

lev.	ux of A $[\times 10^{-3}]$	uy of A $[\times 10^{-3}]$	drag	lift
2	$-3.02 \pm 2.78[10.6]$	$0.99 \pm 35.70[5.3]$	$444.6 \pm 31.69[10.6]$	$9.48 \pm 151.55[5.3]$
3	$-3.02 \pm 2.83[10.6]$	$1.43 \pm 35.43[5.3]$	$457.1 \pm 20.05[10.6]$	$1.23 \pm 146.04[5.3]$
4	$-2.85 \pm 2.56[10.9]$	$1.53 \pm 34.35[5.3]$	$459.8 \pm 20.00[10.9]$	$1.51 \pm 148.76[5.3]$
lev.	ux of A $[\times 10^{-3}]$	uy of A $[\times 10^{-3}]$	drag	lift
2	$-3.00 \pm 2.79[10.7]$	$1.19 \pm 35.72[5.3]$	$445.0 \pm 35.09[10.7]$	$8.26 \pm 163.72[5.3]$
3	$-2.86 \pm 2.68[10.7]$	$1.45 \pm 35.34[5.3]$	$455.7 \pm 24.69[10.7]$	$1.42 \pm 146.43[5.3]$
4	$-2.69 \pm 2.53[10.9]$	$1.48 \pm 34.38[5.3]$	$457.3 \pm 22.66[10.9]$	$2.22 \pm 149.78[5.3]$
ref.	$-2.69 \pm 2.53[10.9]$	$1.48 \pm 34.38[5.3]$	$457.3 \pm 22.66[10.9]$	$2.22 \pm 149.78[5.3]$

Table 15. Results for **FSI3** with timestep $\Delta t = 0.001$, $\Delta t = 0.0005$

5 Summary

The next step will be the specification of how to submit and to collect the results, and the publication of the test configurations in an international journal. Moreover, it is planned to prepare a webpage for collecting and presenting the FSI results. As we have learned from [3], a very important aspect will be the submission of the results on (at least) 3 different meshes and time steps. Then, based on the collected results, quantitative ratings regarding the main questions, particularly w.r.t. the coupling mechanisms and monolithic vs. partitioned approaches, might get possible.

References

1. P. G. Ciarlet. *Mathematical Elasticity. Volume I, Three-Dimensional Elasticity*, volume 20 of *Studies in Mathematics and its Applications*. Elsevier Science Publishers B.V., Amsterdam, 1988.
2. J. Hron and S. Turek. A monolithic FEM/multigrid solver for ALE formulation of fluid structure interaction with application in biomechanics. In H.-J. Bungartz and M. Schäfer, editors, *Fluid-Structure Interaction: Modelling, Simulation, Optimisation*, LNCSE. Springer, 2006.
3. S. Turek and M. Schäfer. Benchmark computations of laminar flow around cylinder. In E.H. Hirschel, editor, *Flow Simulation with High-Performance Computers II*, volume 52 of *Notes on Numerical Fluid Mechanics*. Vieweg, 1996. co. F. Durst, E. Krause, R. Rannacher.
4. W. A. Wall and E. Ramm. Fluid-structure interaction based upon a stabilized (ALE) finite element method. In S. Idelsohn, E. Oñate, and E. Dvorkin, editors, *4th World Congress on Computational Mechanics ? New Trends and Applications*, Barcelona, 1998. CIMNE.